# Influence of Design Parameters on the Effectiveness of Friction Isolators in Mitigating Pre-motion Friction in Mechanical Bearings

Xin Dong, Chinedum E. Okwudire*

Department of Mechanical Engineering, University of Michigan, 2350 Hayward Street, Ann Arbor, MI 48109, USA

*Corresponding author. Tel.: +1 734 647 1531; Fax.: +1 734 647 9379

E-mail address: okwudire@umich.edu (C. E. Okwudire)

## Abstract

Mechanical bearings (i.e., sliding and rolling bearings) are widely used for motion guidance in precision positioning stages due to their low cost, high off-axis stiffness and vacuum compatibility. However, mechanical-bearing-guided stages suffer from the presence of pre-motion (i.e., pre-sliding/pre-rolling) friction which adversely affects their positioning speed and motion precision. The friction isolator has been proposed as a low-cost and robust method for mitigating the undesirable effects of pre-motion friction. It has been experimentally demonstrated that the stage with friction isolator achieves significantly reduced settling times and motion errors in point-to-point positioning and tracking applications, respectively. This paper investigates the influence of design parameters on the effectiveness of friction isolators. Experiments are carried out using three isolators with different parameters to evaluate the settling time and in-position stability during point-to-point motions, and the accuracy and robustness of feedforward friction compensation during circular tracking motions. The experimental results are generalized through numerical simulation and frequency domain analysis with a simple model of a friction-isolated stage under the influence of pre-motion friction. The tradeoffs between different performance

metrics (e.g., precision, speed) are clearly demonstrated. For instance, a friction isolator with lower stiffness and damping coefficient achieves faster settling time; however, the in-position stability of the stage is jeopardized. It is recommended that the friction isolator should be designed with the smallest stiffness while meeting other design requirements such as off-axis rigidity, in-position stability, etc. In addition, critical damping ratio is desired to avoid potential side effects associated with the resonance mode of the friction isolator.

**Keywords**: Pre-sliding friction, pre-rolling friction, bearing, guideway, ultra-precision positioning, tracking control

## 1. Introduction

Motion stages are used for precision positioning in a wide range of manufacturing and metrology-related processes, such as machining, additive manufacturing and semi-conductor inspection, [1], [2]. Mechanical bearings (i.e., sliding and, especially, rolling-element bearings) are commonly used in precision stages due to their long range, high rigidity and ruggedness [1]-[4]. They are also finding increasing use in ultra-precision stages as low-cost alternatives or vacuum compatible substitutes to air bearings [3]-[5]. However, mechanical bearings experience nonlinear friction which adversely affects their positioning precision and speed [1]-[4].

Friction can be divided into two regimes: gross motion (i.e., macro-displacement) and pre-motion (i.e., micro-displacement) regimes, where "motion" implies sliding or rolling [6]-[9]. In the pre-motion regime, friction behaves as a nonlinear spring due to elastoplastic deformation and micro-slip of the inherent rolling elements and end seals of mechanical bearings [3], [4], [10]-[12]. PID-type feedback controllers (e.g., PID, P-PI, etc.) often have difficulties in overcoming high

stiffness and nonlinear change of pre-motion friction, leading to significantly worsened speed and precision, compared to air bearing stages [3], [4], [7]-[14].

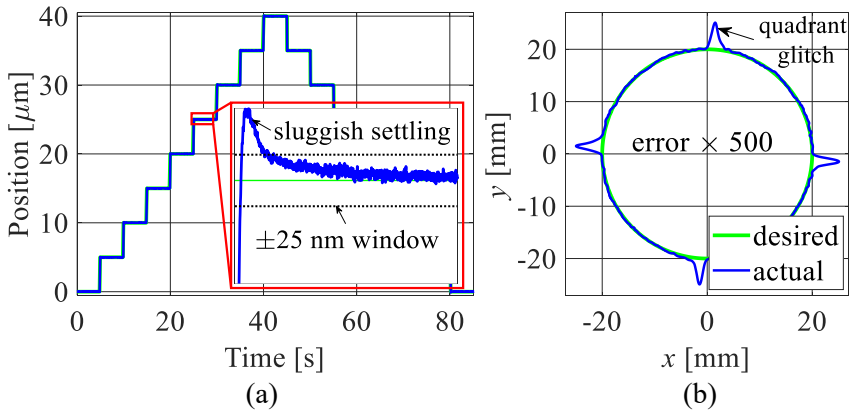


Figure 1. (a) Sluggish settling during point-to-point positioning motion and (b) quadrant glitch during circular tracking motion using a conventional mechanical-bearing-guided motion stage.

During point-to-point positioning motions, the stage is commanded to travel to and settle within a pre-specified window of a target position as fast as possible. Pre-motion friction dominates as the stage approaches its target position, resulting in very sluggish settling performance as shown in Figure 1(a) [3], [4], [10]-[12]. To deal with this problem, PID-type controllers need high gains to quickly overcome the high stiffness of pre-motion friction during settling. However, such high-gain controllers could easily lead to large overshoots, limit cycles and instabilities [3], [4], [10], [15]. Model-based feedback compensation methods are commonly used to mitigate the undesirable effects of pre-motion friction beyond what is achievable using PID-type controllers; some of the examples are nonlinear PID controller, gain scheduling controller, friction observer, etc., [7], [10]-[13], [16], [17]. However, these methods often suffer from robustness and stability problems, since pre-motion friction is extremely nonlinear and variable, thus, limiting their practicality [3], [10].

During tracking motions, the stage is commanded to follow a reference trajectory such as circular or triangular scanning command. Large tracking errors (e.g., glitches) often occur as the PID-type controllers having difficulties to compensate the large frictional stiffness during motion reversals – see Figure 1(b) for an example of quadrant glitch during circular tracking motion [8], [18], [19]. Feedforward friction compensation can significantly reduce quadrant glitches if the friction model employed is accurate enough [18], [20], [21]. However, this often requires the use of complex friction models whose parameters cannot be easily identified [8]. Moreover, feedforward compensators with both simple and complex models of pre-motion friction are not robust to on-machine friction changes that frequently occur as a function of time and/or stage's position [20]-[22]. Thus, they need frequent re-calibration or adaptation to maintain their effectiveness [23].

Apart from the abovementioned control-based compensation methods, a more robust way to reduce the adverse effects of pre-motion friction is through design modifications. For example, a coarse-fine arrangement, where a "fine" flexure stage is stacked on top of a "coarse" rolling bearing stage can be used to improve the precision and speed of mechanical-bearing-guided stage [24], [25]. However, this arrangement makes the system more complex, bulky and expensive [26]. Alternatively, vibration assisted nanopositioning (VAN) has been proposed to improve the settling performance of the ultra-precision stage through high frequency vibration (i.e., dither) [3]. Different from the traditional dithering techniques which jeopardize the motion precision by directly vibrating the stage or guideway [27], [28], VAN is able to mitigate the slow settling problem while maintaining nanometer-level positioning precision [3]. However, the need for additional costly actuators and voltage amplifiers could also limit the practicality of the method.

The friction isolator (FI), also known as the compliant joint method, has recently been proposed as a simple, low-cost and robust method to mitigate the undesirable effects of pre-motion friction [4], [20], [21]. The idea is to connect the mechanical bearing to the moving table of a positioning stage using a joint that is very compliant in the motion direction, thus effectively isolating the stage from the nonlinearities associated with bearing friction. It has been experimentally demonstrated using point-to-point positioning tests that FI makes a PID-type feedback controller to deliver high performance and robustness without the need for very high gains, leading to significantly reduced settling times [4]. Moreover, the addition of FI enables accurate and robust feedforward compensation of pre-motion friction using a simple model, resulting in large and robust reductions of quadrant glitches during circular tracking tests [20], [21]. However, the experimental results so far have been obtained from an ultra-precision motion stage with a proof-of-concept FI design. The influence of design parameters (e.g., stiffness, damping) on the performance of FI, which is critical for applying the method, has not been explored.

Therefore, the key contribution of this paper is in investigating the effects of design parameters on the effectiveness of FI. Specifically, experiments are carried out using three FIs with different stiffness and damping coefficient and the results are generalized through numerical simulation and frequency domain analysis. After a brief overview of the FI concept and experimental setup in Section 2, this paper shows:

1) In Section 3 using point-to-point positioning tests that as the stiffness and damping of FI decrease, the in-position stability becomes worse while the settling performance during short-stroke motions improves significantly. Frequency domain analysis that uses a simple model of the friction-isolated stage under pre-motion friction clearly demonstrates this design tradeoff.

2) In Section 4 using circular tracking tests that the accuracy of feedforward friction compensation improves with lower stiffness and higher damping FI design. Simulation analysis also confirms the experimental observations that the compensator remains robust when the stiffness of FI is an order-of-magnitude smaller than the equivalent stiffness due to pre-motion friction.

This is followed by conclusions and future work in Section 5.

## 2. Overview of Friction Isolator and Experimental Setup

### *2.1. Concept of Friction Isolator*

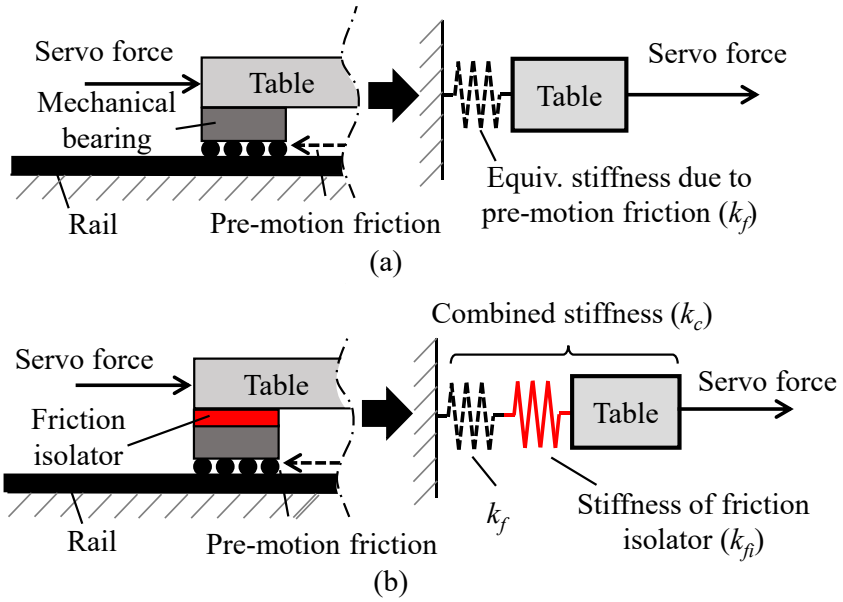


Figure 2. Schematic of a motion stage with bearing (a) rigidly attached to the moving table and (b) attached to the table using a friction isolator (FI).

Figure 2(a) shows the schematic of a conventional motion stage in which the mechanical bearing is rigidly connected to the moving table. Pre-motion friction is modeled as an equivalent

spring of stiffness $k_f$ connecting the table to the ground [3], [4], [6]-[8], [11], [13]. When the stage starts from rest (or after motion reversals), $k_f$ rapidly decreases from its initially large value and eventually becomes zero, such that friction enters the gross motion regime [6], [20]. The large stiffness and highly nonlinear dynamics of pre-motion friction pose great challenges to the PID-type controllers, resulting in severely diminished positioning speed and precision, as discussed in Section 1 [6]-[13], [18]-[21].

Figure 2(b) shows the concept of the friction isolator (FI) for mitigating the undesirable effects of pre-motion friction [4], [20]. Rather than being rigidly attached to the moving table, the bearing is attached using a joint of stiffness $k_{fi}$ in the motion direction. As a result, the friction-isolated stage is modeled statically as a series combination of $k_f$ and $k_{fi}$ with combined stiffness $k_c = k_f k_{fi}/(k_f + k_{fi})$. A very small $k_{fi}$ dominates the combined stiffness felt by the feedback controller when $k_f$ is very large in the pre-motion regime; that is $k_c \rightarrow k_{fi}$ even when $k_f \rightarrow \infty$. Therefore, if $k_{fi} << k_f$ and $k_{fi}$ is precisely known:

1) The PID-type feedback controller can easily suppress the equivalent frictional disturbance without using very high gains, leading to large and robust reductions of settling times during point-to-point motions [4].
2) Accurate and robust feedforward compensation of quadrant glitches can be achieved even when a significant amount of error exists in $k_f$ due to low-fidelity friction modeling or variations of on-machine friction [20], [21].

### *2.2. Experimental Setup: A Friction-Isolated Ultra-Precision Motion Stage*

For the purposes of experimentally investigating the influence of design parameters on the effectiveness of FI, an in-house built ultra-precision motion stage equipped with a FI prototype is

utilized – see Figure 3. The stage has 1.4 kg moving mass and 25 mm travel range. It is guided by a high-rigidity pre-loaded mechanical bearing with end seals (THK, SR-25TB). A voice coil motor (Moticont, LVCM-044), powered by a linear amplifier (Trust Automation, TA-115), is employed to drive the stage. The table position is measured using a linear encoder system (Renishaw, T1000 read head and RGSZ20 scale) with 4.88 nm resolution.

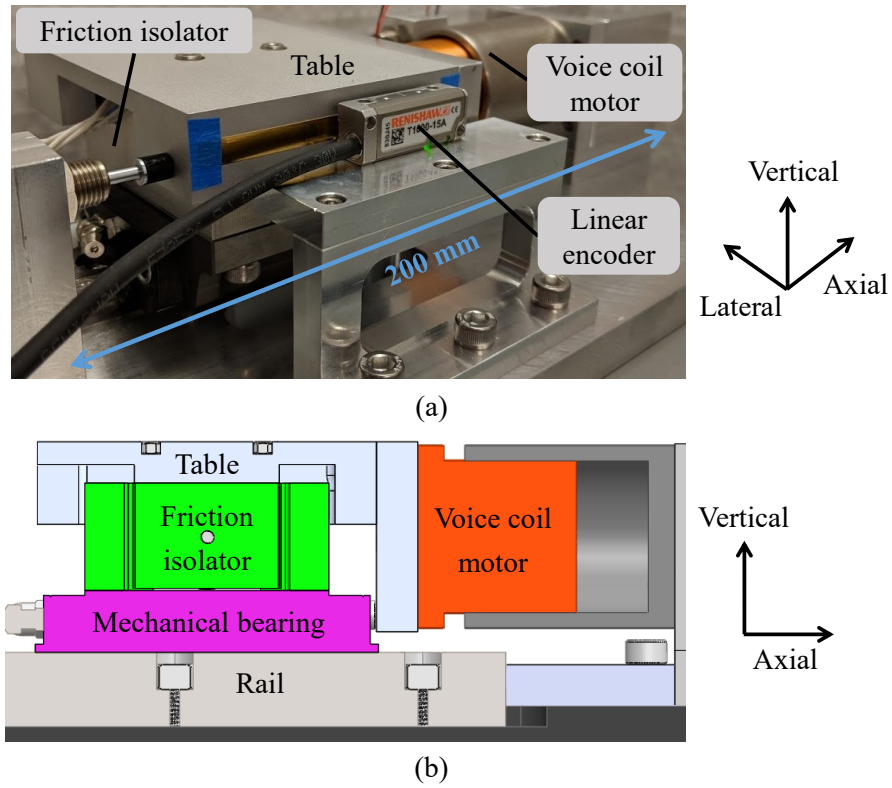


Figure 3. (a) Picture of an ultra-precision motion stage equipped with a FI prototype and (b) cross-section view of the stage's CAD model [29].

A FI prototype designed in [29] is used to attach the mechanical bearing to the moving table of the stage. As shown in Figure 4(a), a flexure with four leaf springs is adopted as the FI, due to its non-contact and friction-free nature. Using two solenoids and permanent magnets (PMs), the designed FI can be switched between two modes: stiff and compliant. When no power is

applied, the PMs attract the ferrous armatures of the solenoids such that the center platform of flexure is locked to the outer platform through contact friction (i.e., the FI is in stiff mode). When power is applied, the solenoids pull the armatures away from the PMs to release the lock (i.e., the FI is in compliant mode). Details of the FI design and manufacture can be found in [29].

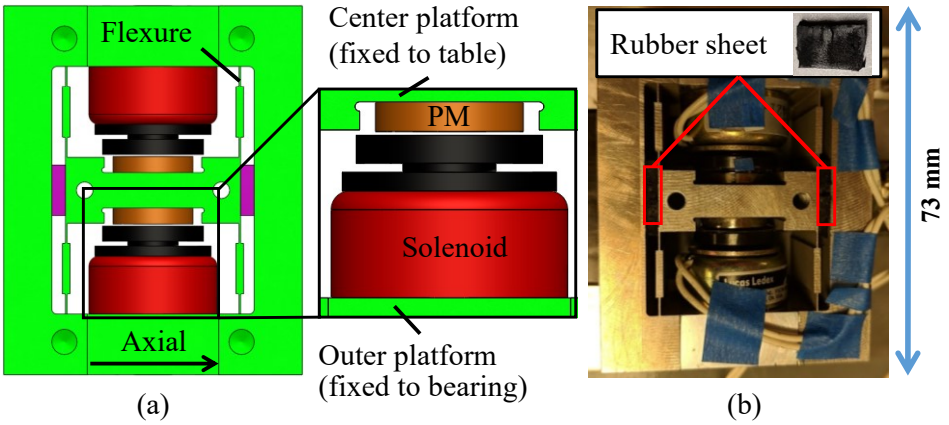


Figure 4. (a) CAD schematic and (b) photo of the FI prototype.

Table 1. Measured parameters of three FIs.

| Test case | Stiffness [N/m] | Damping coefficient [kg/s] |
|---|---|---|
| Low stiffness, low damping (LS-LD) | $3.3 \times 10^4$ | 240 |
| Low stiffness, high damping (LS-HD) | $2.9 \times 10^4$ | 520 |
| High stiffness, high damping (HS-HD) | $6.8 \times 10^4$ | 990 |

Polyurethane rubber sheets with different sizes and hardness are placed in between the center and outer platforms of the flexure to alter the stiffness and damping properties of the designed FI. Table 1 summarizes the measured parameters of the three FIs that are used in the

following experiments. Although the HS-HD case has higher damping coefficient than the LS-HD case, their equivalent damping ratios are similar.

## 3. Influence of Design Parameters on the Effectiveness of FI during Point-to-Point Motion

### *3.1. Point-to-Point Positioning Test*

Experiments are carried out on the ultra-precision stage of Figure 3 to evaluate the effectiveness of FI during point-to-point motions. The stage is given 5 mm and 5 $\mu$m step commands and the time for it to settle into a ±25 nm window after each step is evaluated for the following cases:

1) No FI: the designed FI is always in stiff mode;
2) FI: the designed FI is always in compliant mode.

An industrial-standard PID controller is used to control the motion of the stage. It is tuned to 200 Hz closed-loop bandwidth based on the identified dynamics of the No FI case; the exact same gains are used for controlling the FI case. The feedback controller is implemented on a real-time control board (dSPACE, DS1007).

To illustrate the benefits and potential downsides of FI, Figure 5 compares the settling times and RMS in-position errors of the No FI and FI (HS-HD) cases based on 50 trials at random positions of the table. The mean settling times of the No FI case are 59 ms and 116 ms for the 5 mm and 5 $\mu$m step motions, respectively. The FI case achieves 40% and 49% reductions in the mean settling times, at the costs of 66% and 66% increases of the RMS in-position errors, compared to the No FI case.

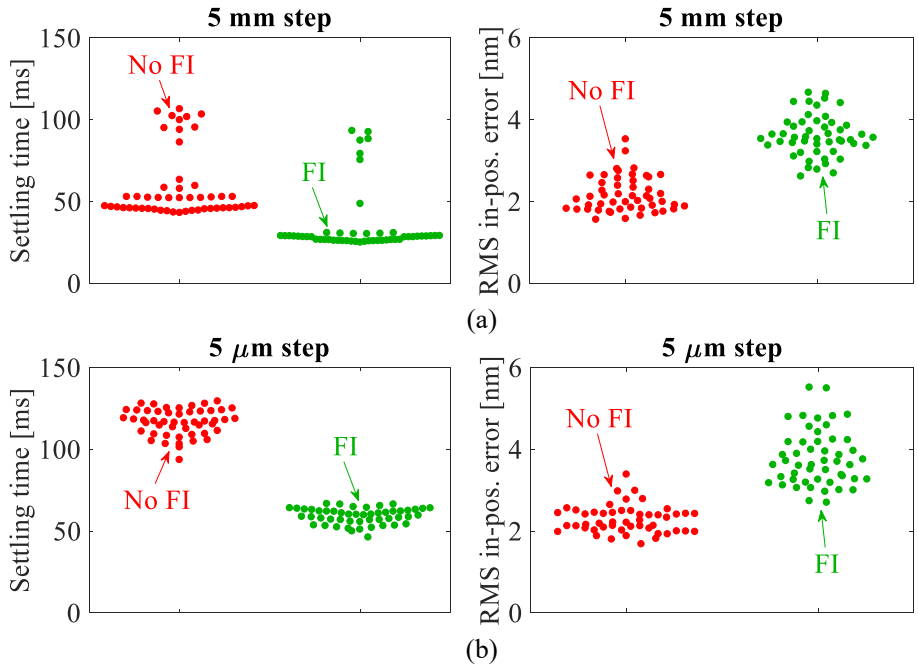


Figure 5. Comparison of RMS in-position error and settling time into a ±25 nm window for No FI and FI (HS-HD) cases during (a) 5 mm and (b) 5 $\mu$m steps.

Table 2. Percentage improvements of settling times and RMS in-position errors using different FIs.

| | | LS-LD | LS-HD | HS-HD |
|---|---|---|---|---|
| 5 mm step | Mean settling time | 36% | 33% | 40% |
| | RMS in-pos. error | –118% | –81% | –66% |
| 5 $\mu$m step | Mean settling time | 89% | 65% | 49% |
| | RMS in-pos. error | –122% | –79% | –66% |

Table 2 summarizes the percentage improvements of settling times and RMS in-position errors of three FIs over the No FI case, during 5 mm and 5 $\mu$m point-to-point positioning tests. The in-position stability improves as the stiffness and damping of the designed FI increase. During 5

$\mu$m step motions, it is observed that the settling time reduces significantly with a FI design of lower stiffness and damping. However, there is no obvious correlation between the settling performance and changes in FI parameters during 5 mm step motions. The following frequency domain analysis is aimed at investigating the influence of design parameters on the settling time and in-position stability of the friction-isolated stage.

### *3.2. Frequency Domain Analysis*

During settling, the stage mainly experiences pre-motion friction, therefore, the servo-controlled stage with FI is represented using the simple model shown in Figure 6. The motion stage is closed-loop controlled through the actuation force $f_a$, using a PID controller. The FI attaching the table of mass $m_t$ to the bearing of mass $m_b$ is modeled by a spring with stiffness $k_{fi}$ and a damper with viscous coefficient $c_{fi}$. Pre-motion friction is also modeled as a spring-damper system of stiffness $k_f$ and damping coefficient $c_f$ that connects the bearing to the fixed ground. In addition, $x_r$, $x_t$ and $x_b$ are, respectively, the reference position, table displacement and bearing displacement. Note that the No FI case can be represented using the same model, assuming rigid connection between the moving table and bearing of the motion stage.

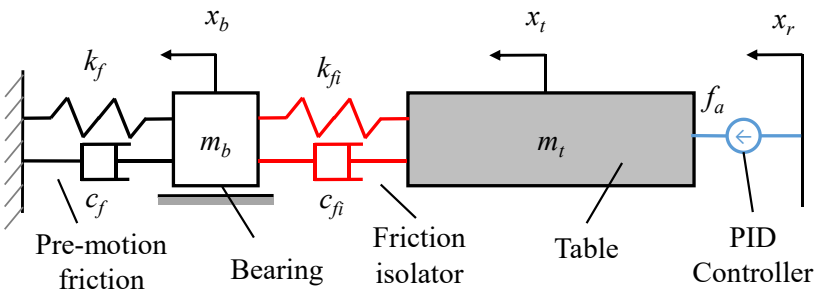


Figure 6. Simple model of a servo-controlled motion stage with FI under the influence of pre-motion friction.

To evaluate the settling performance of the friction-isolated stage, the closed-loop error transfer function $G_e$ is utilized; it is given by

$$G_e = 1 - \frac{x_t}{x_r} = \frac{1}{1+CG} \tag{1}$$

where $C$ and $G$ represent the PID controller and plant dynamics (from input $f_a$ to output $x_t$), respectively

$$\begin{aligned} &C = K_p + \frac{K_i}{s} + K_d s; G = \frac{b_2 s^2 + b_1 s + b_0}{a_4 s^4 + a_3 s^3 + a_2 s^2 + a_1 s + a_0}; \\ &b_2 = m_b; b_1 = c_{fi} + c_f; b_0 = k_{fi} + k_f; \\ &a_4 = m_t m_b;\ a_3 = c_{fi}\left(m_t + m_b\right) + c_f m_t;\ a_2 = k_{fi}\left(m_t + m_b\right) + c_f c_{fi} + k_f m_t; \\ &a_1 = c_f k_{fi} + k_f c_{fi}; a_0 = k_f k_{fi} \end{aligned} \tag{2}$$

where $s$ is the Laplace variable. Figure 7(a) compares the simulated closed-loop error frequency response functions (FRFs) of the friction-isolated stage with the three FIs that are used in experiments. Observe that the FRFs of the FI cases have significantly less magnitudes at lower frequency regions. This is because the combined stiffness is much smaller than that of the pre-motion frictional stiffness, making it easier for the same PID controller to deliver better disturbance rejection. Interestingly, increasing the damping of FI has adverse effects on the magnitude of $G_e$, below the resonance mode due to pre-motion friction (as highlighted in Figure 7(a)) [4][8]. Large damping, especially when the system is overdamped, acts as an additional disturbance that leads to sluggish settling behavior. Figure 7(b) plots the 2-norm of the $G_e$ magnitude over the frequency range from 1 to 50 Hz, which is critical to the settling performance of the stage, as the stiffness and damping coefficient of FI vary. In general, lower stiffness and damping lead to smaller magnitude of closed-loop error FRF and better settling performance, agreeing with the experimental results during 5 $\mu$m step motions. However, observe that reducing the stiffness and

damping beyond certain thresholds (as highlighted in Figure 7(b)) provides little improvements. The frequency domain analysis fails to describe the settling performance during 5 mm point-to-point positioning tests. As the bearing friction experiences transitions between pre-motion and gross motion regimes in a short period of time, complex interactions between friction dynamics, controller dynamics and stage dynamics introduce large uncertainties [30], causing many outliers as seen from Figure 5(a). Therefore, nonlinear analysis is needed to properly understand the transition of friction from pre-motion to gross motion regimes (and vice versa) and its influence on the settling time of long-range point-to-point motion.

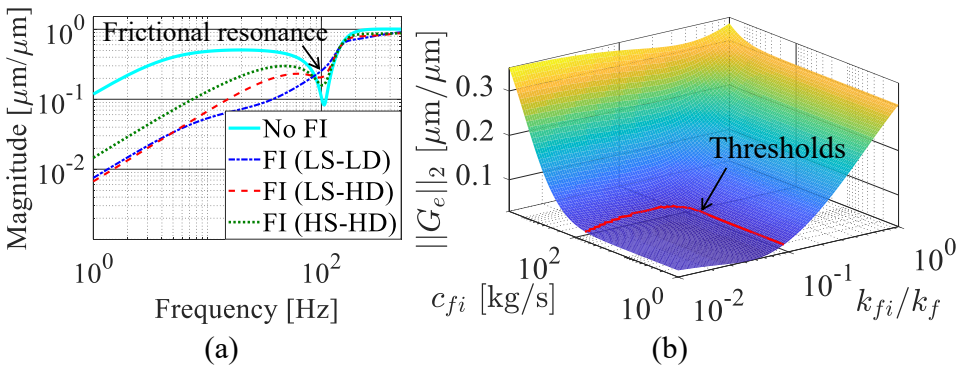


Figure 7. (a) Simulated closed-loop error FRFs and (b) 2-norm of $G_e$ magnitude with different stiffness and damping coefficient of FI.

The in-position stability is analyzed using the closed-loop disturbance transfer function, $G_d$, from motor force to table displacement, since the error is mainly contributed by motor noise during in-position [29]; it is given by

$$G_d = \frac{x_t}{f_a} = \frac{G}{1+CG} \tag{3}$$

Figure 8(a) compares the simulated closed-loop disturbance FRFs using the friction-isolated stage with the three FIs. The FRF of the stage without FI has much smaller magnitudes than that of the

FI cases, because the large frictional stiffness is able to resist the perturbation from motor [29]. Similarly, the FI with higher stiffness has better disturbance rejection ability, thus, smaller in-position error. Increasing damping coefficient attenuates the FRF near the resonance frequency of the FI, leading to better in-position stability. Figure 8(b) summarizes the 2-norm of the $G_d$ magnitude (over the frequency range from 1 to 500 Hz, since motor noise is often broad-band) as a function of the stiffness and damping coefficient. The exact opposite trend as that of Figure 7(b) is observed; high stiffness and damping coefficient lead to smaller magnitude of closed-loop disturbance FRF and smaller in-position error in the presence of motor noise. However, there is no obvious threshold for both design parameters; increasing stiffness and damping results in continuous reduction of $G_d$ magnitude, thus, improving in-position stability.

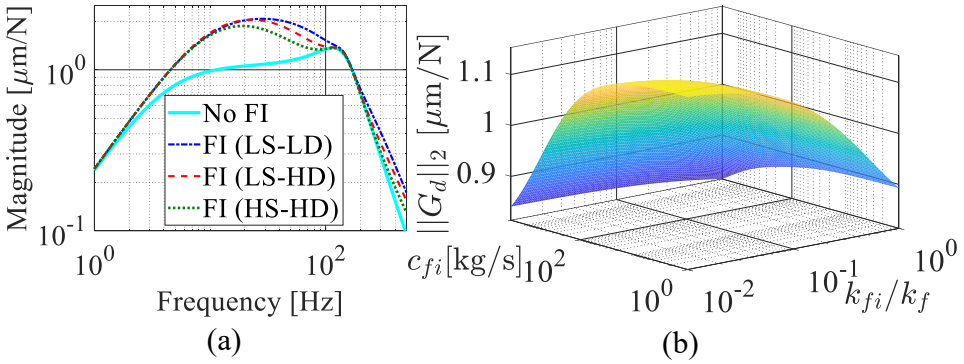


Figure 8. (a) Simulated closed-loop disturbance FRFs and (b) 2-norm of $G_d$ magnitude with different stiffness and damping coefficient of FI.

Given the clear tradeoff between settling performance and in-position stability, careful considerations must be taken when using the FI for point-to-point positioning applications. It is recommended that the FI should be designed to meet the RMS in-position error requirements with the smallest stiffness and damping coefficient. In case the desired in-position stability requirement can be easily achieved with a wide range of parameters, the FI should be designed around the

thresholds to avoid other potential side effects associated with small stiffness and/or damping (e.g., overly sacrificing rigidity in off-motion directions). If no acceptable parameters are found, the designed friction isolator can switch its mode from compliant, during settling, to stiff once the stage gets into position, for simultaneously achieving fast settling and excellent in-position stability (see [29] for details).

## 4. Influence of Design Parameters on the Effectiveness of FI during Point-to-Point Motion

### *4.1. Feedforward Compensation of Pre-Motion Friction*

As discussed in Section 1, feedforward (FF) compensation is often used to mitigate the undesirable effects of pre-motion friction during tracking applications (e.g., quadrant glitches in Figure 1(b)). Figure 9 shows the block diagram of the control scheme with PID feedback controller and model-based FF friction compensator. Two popular pre-motion friction models are used in the FF friction compensator, namely the Dahl and generalized Maxwell-slip (GMS) models.

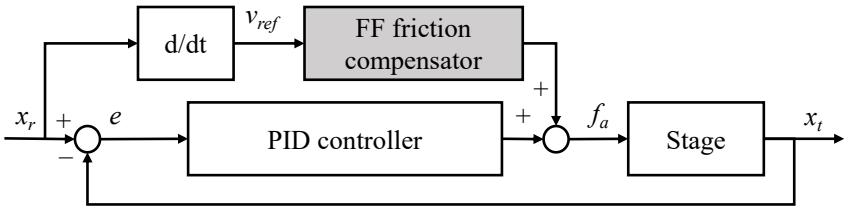


Figure 9. Block diagram of the control scheme with PID controller and model-based feedforward (FF) friction compensator.

Table 3. Identified Dahl friction model parameters (No FI case).

| $f_C$ [N] | $k_\sigma$ [N/m] |
|---|---|

| | |
|---|---|
| 4.3 | $5 \times 10^5$ |

Table 4. Identified GMS friction model parameters (No FI case).

| $i$ | $k_i$ [N/m] | $\alpha_i$ | $i$ | $k_i$ [N/m] | $\alpha_i$ |
|---|---|---|---|---|---|
| 1 | $3.9 \times 10^5$ | 0.0104 | 6 | $4.9 \times 10^4$ | 0.0961 |
| 2 | $4.6 \times 10^4$ | 0.0605 | 7 | $1.4 \times 10^4$ | 0.0448 |
| 3 | $2.3 \times 10^4$ | 0.0916 | 8 | $2.2 \times 10^4$ | 0.1055 |
| 4 | $1.7 \times 10^4$ | 0.1333 | 9 | $3.1 \times 10^4$ | 0.2025 |
| 5 | $1.1 \times 10^4$ | 0.1453 | 10 | $1.4 \times 10^4$ | 0.1100 |

The Dahl friction model [11] is the simplest model that predicts the spring-like characteristic of pre-motion friction. It is described by

$$f_f = k_\sigma z; \frac{dz}{dt} = \dot{x}\left(1 - \frac{f_f}{f_C}\right) \tag{4}$$

where $f_f$ is the friction force, $k_\sigma$ is the initial frictional stiffness, $f_C$ is the Coulomb friction force, $x$ is the relative displacement between frictional surfaces and $z$ is an internal state of friction dynamics.

Due to the limited tuning parameters, Dahl model often fails to accurately capture the complex dynamics of pre-motion friction [20], [21]. Therefore, advanced models like the GMS model have been developed [6]. The GMS model consists of $N$ elementary (massless) blocks and springs connected in parallel. The behavior of each elementary block is determined by two states (i.e., stick or slip) and is represented by

$$f_f = \sum_{i=1}^{N} f_i;\ \ \frac{df_i}{dt} = \begin{cases} k_i \dot{} & (\text{i.e.}, f_i < \alpha_i f_C) \\ 0, \text{if slip } (\text{i.e.}, f_i = \alpha_i f_C) \end{cases};\ \ \frac{dz}{dt} = \dot{} \tag{5}$$

where $f_i$, $k_i$ and $\alpha_i$ are the friction force, spring stiffness and saturation limit of the $i$th GMS block; the internal frictional state $z$, is shared by all blocks. Table 3 and Table 4 summarize the measured Dahl and GMS model parameters of the stage with FI. Note that the equivalent parameters of the FI cases are calculated by combining frictional stiffness and FI stiffness in series. Details of the friction models and identification of their parameters can be found in [20].

### *4.2. Circular Tracking Tests*

The effectiveness of FI is experimentally evaluated using circular tracking tests with 5 mm and 5 $\mu$m radius and different tangential velocities. Since the ultra-precision stage is a single-axis stage, without loss of generality, only the $x$-axis reference trajectories of the circular motions are utilized. The following cases are tested:

1) Baseline: No FI case without FF compensation;
2) No FI + Dahl: No FI case with Dahl FF compensation;
3) No FI + GMS: No FI case with GMS FF compensation;
4) FI + Dahl: FI case with Dahl FF compensation;
5) FI + GMS: FI case with GMS FF compensation.

Note that deviations of 0, ±10%, ±20%, ±50% are introduced in the identified frictional stiffness of the No FI case (as summarized in Table 3 and Table 4), to test the robustness of FF compensator in the presence of model parameter errors. For each deviation case, the equivalent stiffness parameters of the FI case are re-calculated using the inaccurate frictional stiffness (see [20] for more details).

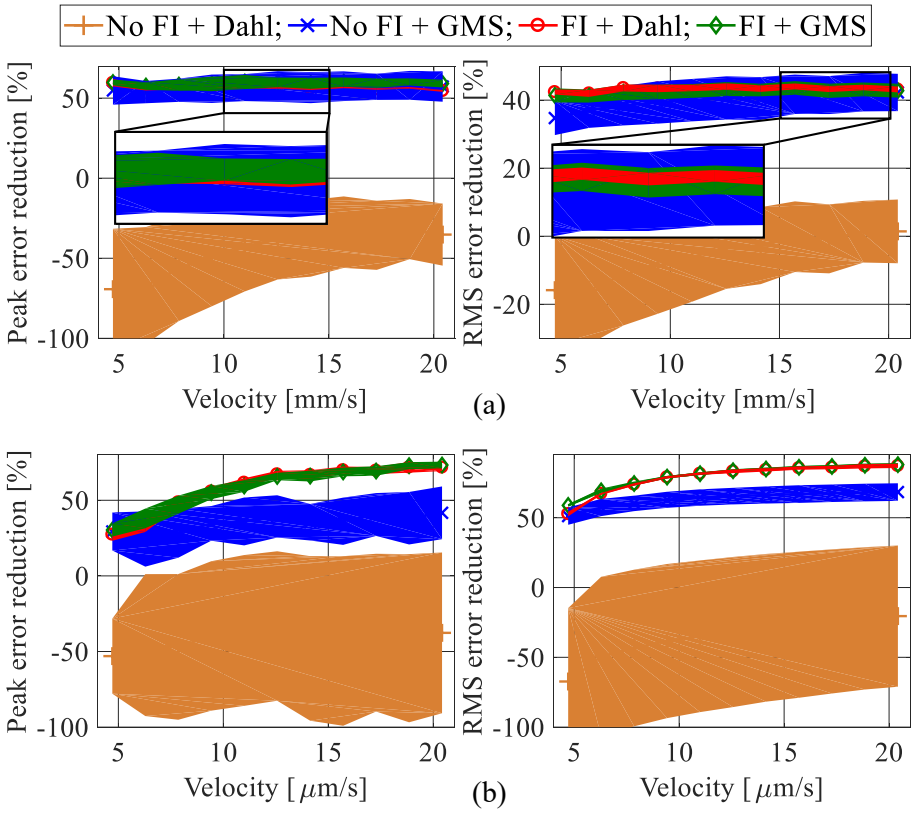


Figure 10. Comparison of tracking performance during circle tests of (a) 5 mm and (b) 5 $\mu$m radius. Solid lines represent mean values and shaded bands indicate $\pm 1\sigma$ (standard deviation).

Figure 10 summarizes the percentage reductions in peak and RMS tracking errors achieved by different methods, relative to the baseline case; note that HS-HD design is used in the FI case. The performance variations are also compared by plotting the mean percentage reductions together with the corresponding $\pm 1\sigma$ (standard deviation) bands based on all deviation cases for each method. No FI + Dahl and No FI + GMS both suffer from large performance variations due to the modeling errors in their identified pre-motion frictional parameters. This indicates that frequent re-calibration is needed to ensure robust FF compensation of quadrant glitches for the No FI case. On the other hand, FI + Dahl provides very robust tracking performance due to using the combined stiffness $k_c$ in the FF compensator that is more linear and less variable. With the FI, accurate and

robust compensation of pre-motion friction is achieved in the presence of up to 50% errors in the identified frictional stiffness. GMS model is also used in the FI case and the resulting percentage improvements of peak and RMS errors are very similar or only slightly better, compared to that of the FI + Dahl case.

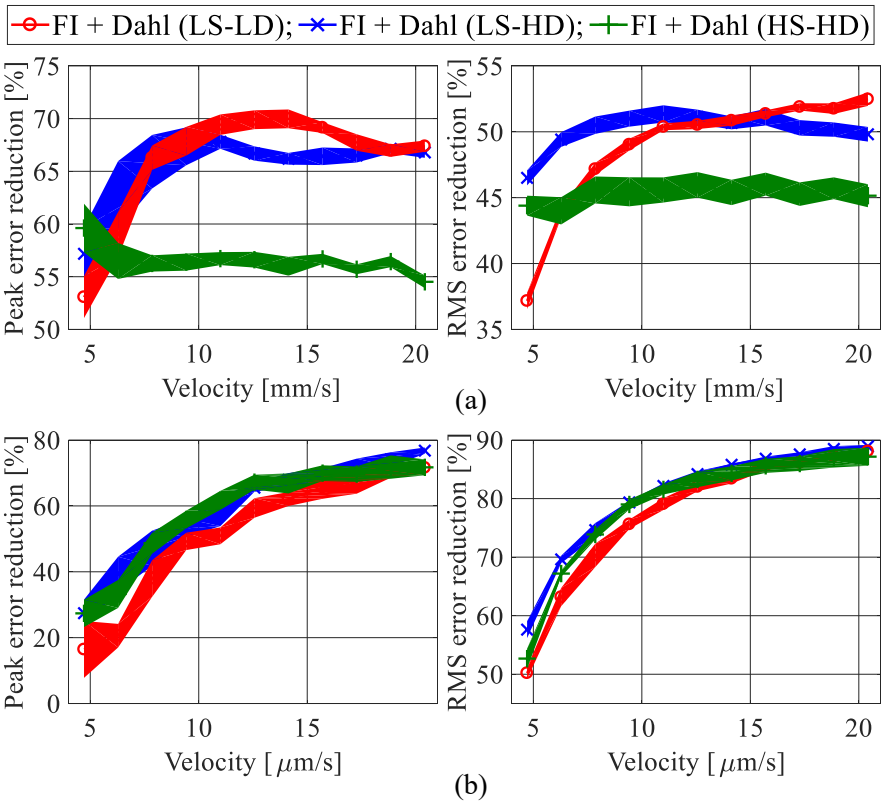


Figure 11. Comparison of tracking performance during circle tests of (a) 5 mm and (b) 5 $\mu$m radius. Solid lines represent mean values and shaded bands indicate $\pm 1\sigma$ (standard deviation).

Figure 11 compares the percentage error reductions in peak and RMS tracking errors achieved by different FI designs (over the baseline case). Note that only the results of Dahl FF compensation are plotted since using the complex GMS model in the compensator does not lead to significant improvements over the simple Dahl model. Regardless of the changes in stiffness and damping coefficient, the robustness of FF compensator for the three FIs are very similar; the

remaining variations are mainly due to non-repeatable disturbances in the system, such as motor noise, variations of on-machine friction dynamics. Also observe that FF compensation using the three FIs achieves almost the same performance during circle tests of 5 $\mu$m radius. In this case, the FI behaves as a linear low-stiffness spring, which dominates the equivalent stiffness felt by the servo controller; the accuracy of FF compensator remains un-affected if the identified FI stiffness is accurate enough. As the stiffness of FI increases, the effectiveness of FF compensator during circle tests of 5 mm radius becomes worse; however, the differences of peak and RMS error reductions are only about 10% and 5%, respectively. Interestingly, reducing the damping coefficient of FI negatively impacts the RMS error reductions, especially during circle tests with lower velocities. This is because the tracking errors during non-motion reversal portions of the circle, which are mainly contributed by the variations of gross motion friction [31], have large impacts on the overall RMS errors. The resonance mode due to the FI can be easily excited when the damping is small, resulting in increased motion errors [31]. The benefits of higher damping on the RMS tracking errors vanish when the reference velocity is large, as the peak errors during motion reversals become dominant.

### *4.3. Simulation Analysis*

As discussed in the previous section, the accuracy and robustness of FF friction compensation are primarily affected by the stiffness of FI. As shown in Figure 10, the performance of FI + Dahl is very similar to that of FI + GMS. So it makes practical sense to use the simpler model with the FI. Therefore, in this section, the accuracy of FI + Dahl is evaluated against FI + GMS to understand under what circumstances the FI can enable accurate FF compensation using

the simple Dahl model. It is assumed that, due to its high order, the GMS model can accurately capture the actual friction dynamics of the stage if its parameters are carefully identified.

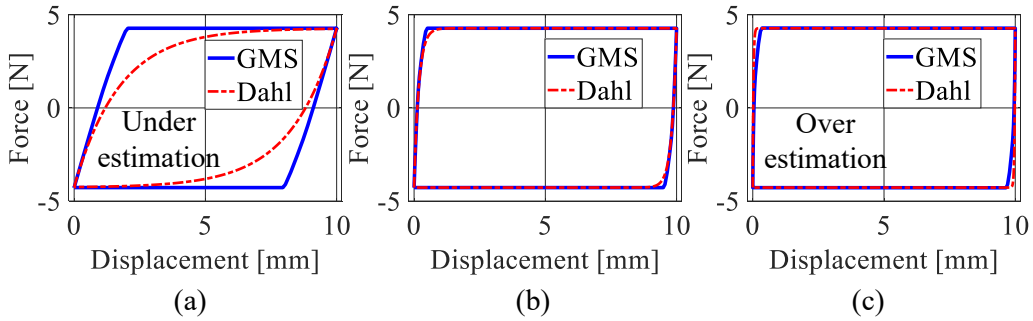


Figure 12. Simulated frictional forces using Dahl and GMS models for the FI case with stiffness ratio ($k_{fi}/k_f$) of (a) 0.01, (b) 0.1 and (c) 1.

Figure 12 compares the simulated friction forces during 5 mm radius circle test using Dahl and GMS models for the FI case with different stiffness; note that the tangential velocity is irrelevant since both friction models are rate-independent. In general, smaller stiffness leads to more linear behavior of the combined stiffness and better compensation accuracy. However, Dahl model tends to underestimate the friction force when the FI stiffness is extremely small, resulting in large RMS force difference. Fortunately, the feedback controller has the ability to effectively suppress this slow change of disturbance force. Figure 13(a) plots the calculated RMS force difference, $\gamma$, between Dahl and GMS models for the FI case during one cycle of the 5 mm circle test. The accuracy of FF compensator using the Dahl model is optimal when the stiffness ratio ($k_{fi}/k_f$) is around 0.05 – 0.1. Increasing the stiffness of FI beyond this range often leads to over-compensation of the friction force, which is commonly observed in the stage without FI as error spikes toward the opposite direction of stage's motion [20], [21].

The robustness of FF compensator is investigated through static stiffness analysis, using the stage's model shown in Figure 2. The sensitivity $\kappa$ of the combined stiffness $k_c$ to errors in $k_f$ (due to low fidelity model or variations of friction) can be calculated as

$$\kappa = \frac{\partial k_c}{\partial k_f} = \left( \frac{\eta}{1+\eta} \right)^2, \quad \text{where } \eta = \frac{k_{fi}}{k_f} \tag{6}$$

Note that if $k_{fi} << k_f$, and $k_{fi}$ is precisely known, $\eta \to \infty$ and $\kappa \to 0$. This indicates that if FF compensation is carried out using the FI case (i.e., $k_c$), variations of $k_f$ will not affect the result much. Figure 13(b) plots the sensitivity $\kappa$ as the stiffness ratio $\eta$ changes. So long as the stiffness of FI is one order-of-magnitude smaller than that of the equivalent stiffness of pre-motion friction (i.e., $\eta < 0.1$), the FF compensation remains relatively robust.

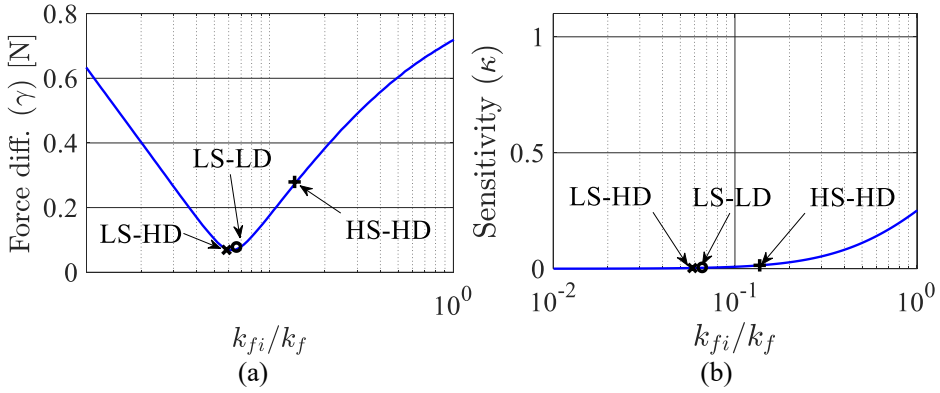


Figure 13. (a) Calculated RMS force difference ($\gamma$) between Dahl and GMS models for the FI case during circle test of 5 mm radius and (b) sensitivity of combined stiffness $k_c$ to variations of frictional stiffness $k_f$.

Since the accuracy and robustness of FF friction compensation both improve as the stiffness of FI reduces, using FI for tracking applications is more straightforward. It is recommended that the FI should be designed to have as small stiffness as possible. In practice, this

is often limited by other design considerations, such as the off-axis stiffness requirements. The damping of FI should be designed to achieve at least a critically damped system to avoid excitation of the resonance mode by variations of friction force in the gross motion regime [31], or other un-modeled disturbances.

## 5. Conclusions and Future Work

Friction isolator (FI) has recently been proposed as a simple, robust and effective method for mitigating the undesirable effects of pre-motion friction on the positioning speed and precision of mechanical-bearing-guided motion stage. The motion stage with the FI (i.e., friction-isolated stage) has achieved greatly reduced settling times and motion errors during point-to-point positioning and circular tracking tests, respectively. This paper has investigated the influence of design parameters on the effectiveness of friction isolator. An ultra-precision stage with a FI prototype was used for experimental validation; the stiffness and damping coefficient of the designed FI were varied by adding rubber sheets of different sizes and hardness.

During point-to-point positioning tests, a clear tradeoff between faster settling and better in-position stability was observed for short-range motions: the stage with a lower stiffness and damping FI design achieves better settling performance at the cost of increased in-position error. Frequency domain analysis using a simple model of the friction-isolated stage under the influence of pre-motion friction confirmed the experimental findings. When using FI for point-to-point positioning applications, it should be designed to meet the in-position stability requirement with the smallest stiffness and damping coefficient.

During circular tracking tests, accurate and robust feedforward (FF) compensation of pre-motion was achieved in the presence of up to 50% modeling errors (or variations) in the identified

frictional stiffness. Sensitivity analysis with respect to variations of friction revealed that the FF compensator remains robust so long as the stiffness of FI is an order-of-magnitude smaller than the initially large value of pre-motion frictional stiffness. The accuracy of FF compensation also improves when the stiffness of FI reduces, as was confirmed by both numerical simulation and experiments. When using FI for tracking applications, its stiffness should be designed as small as possible with a large enough damping coefficient. Other design requirements should also be considered in practice, such as the off-axis rigidity of the stage.

Due to the nonlinear transitions of friction between pre-motion and gross motion regimes, the frequency domain analysis in Section 3 is not capable of describing the settling behavior of the friction-isolated stage during 5 mm step motions. Future work will focus on understanding the complex interactions between friction dynamics and servo dynamics through nonlinear analysis, thus predicting the settling performance during long-range positioning (see [30] for preliminary dynamical analysis). A systematic framework will then be proposed for optimal design of the FI, based on different performance metrics (e.g., settling time, tracking error, etc.) and practical design constraints (e.g., dimension, off-axis stiffness, etc.)

**Acknowledgements**

This work is funded by National Science Foundation Award [grant number CMMI #1855354]: Towards a Fundamental Understanding of a Simple, Effective and Robust Approach for Mitigating Friction in Nanopositioning Stages.

**References**

[1] Altintas Y, Verl A, Brecher C, Uriarte L, Pritschow G. Machine tool feed drives. CIRP Ann - Manuf Technol 2011;60:779–96. https://doi.org/10.1016/j.cirp.2011.05.010

[2] Amin-Shahidi D, Trumper D. Macro-scale atomic force microscope: an experimental platform for teaching precision mechatronics. Mechatronics 2015;31:234-42. https://doi-org.proxy.lib.umich.edu/10.1016/j.mechatronics.2015.08.007

[3] Dong X, Yoon D, Okwudire CE. A novel approach for mitigating the effects of pre-rolling/pre-sliding friction on the settling time of rolling bearing nanopositioning stages using high frequency vibration. Precis Eng 2017;47:375–88. https://doi.org/10.1016/j.precisioneng.2016.09.011

[4] Dong X, Okwudire CE. An experimental investigation of the effects of the compliant joint method on feedback compensation of pre-sliding/pre-rolling friction. Precis Eng 2018;54:81–90. https://doi.org/10.1016/j.precisioneng.2018.05.004

[5] Sitti M. Survey of nanomanipulation systems. Proc. the 1st IEEE Conf. Nanotechnology., IEEE; 2001, p. 75–80. doi:10.1109/NANO.2001.966397

[6] Al-Bender F, Swevers J. Characterization of friction force dynamics. IEEE Control Syst Mag 2008;28:64–81. doi:10.1109/MCS.2008.929279

[7] Maeda Y, Iwasaki M. Initial friction compensation using rheology-based rolling friction model in fast and precise positioning. IEEE Trans Ind Electron 2013;60:3865–76. doi:10.1109/TIE.2012.2205350

[8] Yoon JY, Trumper DL. Friction modeling, identification, and compensation based on friction hysteresis and Dahl resonance. Mechatronics 2014;24:734–41. https://doi.org/10.1016/j.mechatronics.2014.02.006

[9] Ruderman M. On break-away forces in actuated motion systems with nonlinear friction. Mechatronics 2017;44:1–5. https://doi.org/10.1016/j.mechatronics.2017.03.007

[10] Armstrong-Hélouvry B, Dupont P, Canudas de Wit C. A survey of models, analysis tools and compensation methods for the control of machines with friction. Automatica 1994;30:1083–138. https://doi.org/10.1016/0005-1098(94)90209-7

[11] Bucci B, Vipperman J, Cole D, Ludwick S. Evaluation of a servo settling algorithm. Precis Eng 2013;37:10–22. https://doi.org/10.1016/j.precisioneng.2012.04.006

[12] Ruderman M. Presliding hysteresis damping of LuGre and Maxwell-slip friction models. Mechatronics 2015;30:225–30. https://doi.org/10.1016/j.mechatronics.2015.07.007

[13] Futami S, Furutani A, Yoshida S. Nanometer positioning and its micro-dynamics. Nanotechnology 1990;1:31–7. https://doi.org/10.1088/0957-4484/1/1/006

[14] Lin T, Pan Y, Hsieh C. Precision-limit positioning of direct drive systems with the existence of friction. Control Eng Pract 2003;11:233–44. https://doi.org/10.1016/S0967-0661(02)00110-7

[15] Chong S, Sato K. Practical controller design for precision positioning, independent of friction characteristic. Precis Eng 2010;34:286–300. https://doi.org/10.1016/j.precisioneng.2009.09.006

[16] Kim H, Park S, Han S. Precise friction control for the nonlinear friction system using the friction state observer and sliding mode control with recurrent fuzzy neural networks. Mechatronics 2009;19:805–15. https://doi.org/10.1016/j.mechatronics.2009.04.004

[17] Keck A, Zimmermann J, Sawodny O. Friction parameter identification and compensation using the ElastoPlastic friction model. Mechatronics 2017;47:168–82. https://doi.org/10.1016/j.mechatronics.2017.02.009

[18] Jamaludin Z, Van Brussel H, Swevers J. Friction compensation of an xy feed table using friction-model-based feedforward and an inverse-model-based disturbance observer. IEEE Trans Ind Electron 2009;56:3848–53. doi:10.1109/TIE.2009.2017560

[19] Ruderman M. Tracking control of motor drives using feedforward friction observer. IEEE Trans Ind Electron 2014;61:3727–35. doi:10.1109/TIE.2013.2264786

[20] Dong X, Liu X, Yoon D, Okwudire CE. Simple and robust feedforward compensation of quadrant glitches using a compliant joint. CIRP Ann - Manuf Technol 2017;66:353–6. https://doi.org/10.1016/j.cirp.2017.04.048

[21] Dong X, Okwudire CE. Detailed experimental evaluation of the compliant joint method for feedforward compensation of pre-motion friction. Proc. - 32rd ASPE Annu. Meet.; 2017.

[22] Miura T, Matsubara A, Yamaji I, Hoshide K. Measurement and analysis of friction fluctuations in linear guideways. CIRP Ann - Manuf Technol 2018;67:393–6. https://doi.org/10.1016/j.cirp.2018.04.010

[23] Dumanli A, Sencer B. Pre-compensation of servo tracking errors through data-based reference trajectory modification. CIRP Ann - Manuf Technol 2019;68:397–400. https://doi.org/10.1016/j.cirp.2019.03.017

[24] Elfizy A, Bone G, Elbestawi M. Design and control of a dual-stage feed drive. Int J Mach Tools Manuf 2005;45:153–65. https://doi.org/10.1016/j.ijmachtools.2004.07.008

[25] Juhász L, Maas J. Control of hybrid nanopositioning systems for trajectory-tracking applications. Mechatronics 2013;23:617–29. https://doi.org/10.1016/j.mechatronics.2013.06.008

[26] Awtar S, Parmar G. Design of a large range xy nanopositioning system. J Mech Robot 2013;5:021008 1-10. https://doi.org/10.1115/DETC2010-28185

[27] Engel T, Lechler A, Verl A. Sliding bearing with adjustable friction properties. CIRP Ann - Manuf Technol 2016;65:353–6. https://doi.org/10.1016/j.cirp.2016.04.084

[28] Tanaka T, Oiwa T, Syamsul H. Positioning behavior resulting from the application of ultrasonic oscillation to a linear motion ball bearing during step motion. Precis Eng 2017;51:362–72. https://doi.org/10.1016/j.precisioneng.2017.09.007

[29] Dong X, Okwudire CE. Semi-active joint for ultra-precision positioning using sliding/rolling bearings. CIRP Ann - Manuf Technol 2019;68:385–8. https://doi.org/10.1016/j.cirp.2019.04.021

[30] Wang J, Dong X, Barry O, Okwudire CE. Dynamical analysis of friction induced vibration in a precision motion stage with a friction isolator. arXiv preprint; 2019.

[31] Kang D, Dong X, Kim H, Park P, Chinedum CE. Friction isolated rotary system for high-precision roll-to-roll manufacturing. Proc. - 34th ASPE Annu. Meet.; 2019.